Geological Magazine

www.cambridge.org/geo

Methods for determining the characteristics of weathered granite reservoirs: application to Binxian Uplift, Dongying Sag, Bohai Bay Basin

Xiaoke Li[1], Gang Chen[1] and Shangzi Liang[2]

[1]State Key Laboratory of Continental Dynamics, Department of Geology, Northwest University, Xi'an, 710069, China and [2]State Key Laboratory of Petroleum Resources and Prospecting in China University of Petroleum, Beijing, 102249, China

Original Article

Cite this article: Li X, Chen G, and Liang S (2022) Methods for determining the characteristics of weathered granite reservoirs: application to Binxian Uplift, Dongying Sag, Bohai Bay Basin. *Geological Magazine* **159**: 1727–1743. https://doi.org/10.1017/S001675682200053X

Received: 9 October 2021
Revised: 27 April 2022
Accepted: 10 May 2022
First published online: 19 July 2022

Keywords:
granite; weathering; fractured basement reservoir; Archean; Binxian Uplift

Author for correspondence:
Gang Chen, Email: chengang201206@163.com

Abstract

With the discovery of high-productivity oilfields in granite buried hills, it is necessary to systematically investigate the types of granite weathered reservoirs at different depths and their spatial distribution. However, previously subdivided reservoirs have been assumed to exhibit the same vertical zoning in different structural parts, contradicting the fact that the degree of weathering varies with the topography. In addition, comprehensive and quantitative methods for classifying reservoir types are lacking. Taking the Binxian Uplift of the Dongying depression in Bohai Bay Basin as an example, we therefore established a comprehensive identification standard for dividing granite reservoirs using lithology division, logging curve statistics, a dual-medium matrix–fracture model and seismic facies identification. Subsequently, by combining logging and seismic methods, the vertical stacking types and distribution properties of weathered granite reservoirs in various structural positions were analysed. The reservoirs were divided vertically into three zones: regolith, dissolution and fracture. Quantitative logging response standards for the different reservoirs were established using acoustic, density, natural gamma and resistivity logging. In terms of the seismic response, the regolith, dissolution and fracture zone corresponded to high-, medium- and low-amplitude seismic facies, respectively. A dynamic double-layer structure of the reservoir was established, comprising a completely weathered layer and a semi-weathered layer. The reservoir division method proposed in this paper can be used in other areas, and the research results can help promote the exploration of granite buried hill reservoirs.

1. Introduction

As a frontier subject in unconventional exploration, granite buried hills are being explored for increased oil and gas production. In the oil and gas industry, granite buried hills have been found in ancient bedrock platforms (North and South America) (Koning, 2003; Sorenson, 2005), young platforms (West Siberia, Western Europe) (Trice, 2014; Belaidi *et al.* 2018; Holdsworth *et al.* 2019) and young fold mountain belt depressions (Venezuela) (Nelson *et al.* 2000). Approximately 40% of oil and gas is produced from weathered granite reservoirs, and their reserves account for approximately 75% of reserves in the entire base rock oil and gas field (Williams & Augifield, 1972; Trinh *et al.* 2009). Representative examples include Venezuela's La Paz field and Vietnam's Baihu oilfield (Koning, 2003; Borgohain, 2010; Haskell *et al.* 2010; Li, 2011), which belong to a tertiary granitic basement reservoir with reserves of over 3.7 billion barrels and a daily production of over 6000 barrels. The exploration of weathered granite reservoirs has also yielded some good results in China; examples include Penglai 9-1, Jinzhou 25-1S, Niuxintuo granite buried hill, Xinglongtai granite buried hill and Chengbei 30 buried hill (Wang *et al.* 2006; Deng, 2007; Cun, 2008; Shi *et al.* 2008; Fang, 2016). With the discovery of several weathered granite reservoirs in the Bohai Bay Basin, it is necessary to thoroughly study such reservoirs for higher oil and gas production. Moreover, as fractured reservoirs, they can be used to build deep nuclear waste and CO_2 storage warehouses, which play an important role in reducing greenhouse gas emissions and avoiding nuclear pollution (Armitage *et al.* 2013; Hung *et al.* 2019).

Because a granite buried hill has undergone varying degrees of weathering and has strong heterogeneity, evident zones are formed in the vertical direction. Based on the proportion of the main minerals, the type of storage space and the density of fracture development in a weathered granite reservoir, it can be divided into different zones from top to bottom, that is, soil, sandy weathering zone, gravel weathering zone, and fractured and bedrock zone; alternatively, it can be divided into weathered and leached, fractured, semi-filled fractured and tight zones (Dou *et al.* 2015, 2018; Wang *et al.* 2015, 2018). As the depth increases, the type of reservoir space gradually transitions from mainly pores to fractures (Deng & Peng, 2009; Zhou,

2016). With gradually increasing depth, the permeability and porosity vary significantly in the vertical direction. The porosity decreases from 4% to 1%, and the permeability decreases from 13 mD to 0.1 mD (Chen *et al.* 2009; Ge *et al.* 2011). Based on imaging logging, cores, thin slices, outcrops and other data, geostatistics or artificial neural network methods have been used to analyse the physical properties of fractured reservoirs (Nguyen-Trinh & Ha-Duong, 2015; Riber *et al.* 2017; Bonter & Trice 2019; Liu *et al.* 2020). Further, the normalized correlation count method has been used to analyse the spatial distribution of fractures (Wang *et al.* 2019). To identify the structure of the weathering crust and its distribution, numerous attempts have been made through logging and seismic analyses. The non-conductivity of a granitic framework is characterized by its high resistance response. The phenomenon of 'cycle jumping' of the acoustic logging data reflects the development of fractures in the basement rock (Ni *et al.* 2015; Tan *et al.* 2015). In terms of the seismic response, high-frequency and strong-amplitude reflections mostly correspond to a weathered zone, and chaotic or blank reflections correspond to a basement dense zone. Messy or blank reflections correspond to the dense zone of basement rocks (Huang *et al.* 2007; Li *et al.* 2009; Gong, 2010). The formation and distribution of weathered granite reservoirs are affected to a certain extent by leaching, denudation time, palaeo-climatic environment, lithological differences and tectonic evolution (Huang *et al.* 2016; Place *et al.* 2016; Trice *et al.* 2019; Alberto *et al.* 2021).

Despite knowing that a weathered granite reservoir has evident vertical zoning, studies have not yet developed a quantitative and comprehensive classification scheme. The unified weathering crust division plan for the entire region neglects the objective fact that the weathering crust structure varies with the change in the structural position. It is therefore necessary to consider the differences in the distribution of the weathering crust structures in the different parts of a buried hill during topographic and structural changes, but also the configuration relationship of the vertical zoning at different locations. Finally, the formation, destruction and preservation of weathered granite reservoirs are dynamic evolutionary processes. The existing static division mode does not consider the influence of reservoir reconstruction and preservation on its distribution, which increases the uncertainty in the exploration of granite reservoirs.

In this study, a classification scheme for weathered granite reservoirs was established through core observations, logging data, physical property calculations and seismic facies analysis. By applying the classification scheme to each studied well and analysing the correlations between wells, vertical zoning characteristics of the studied reservoir were identified. The stacking relationship of the reservoirs in different structural positions was analysed, and the spatial distribution of the reservoirs were clarified. In addition, the factors controlling the later preservation of the reservoirs were determined and an oil-bearing analysis of the reservoirs was conducted. The novelty of this research lies in the use of the dual-medium matrix–fracture model to determine the physical properties of the reservoirs, combined with logging data statistics and seismic analysis to establish a quantitative identification standard for the different weathered granite reservoirs in the study area. Unlike the existing fixed reservoir structure, three types of vertical stacking relationships were established based on the reservoir distribution at various structural positions. The factors influencing the reconstruction and preservation of the weathered granite reservoirs were also discussed. The results provide a theoretical basis and guidance for the global exploration of granite reservoirs.

2. Geological setting

The study area is located in Binzhou City, Shandong Province in the territory of Lijin County, Dongying City. The structural location is above the Binxian Uplift in Dongying Sag, Bohai Bay Basin, located in the west of Dongying Sag with the Chenjiazhuang Uplift to the north, the Lijin oil-generating Sag to the east and the Binnan Fault to the south. The Archean bedrock in the Binxian area is an inherited uplift from the end of the Mesozoic Era (Fig. 1a). The seismic profile shows that the main body of the Binxian Uplift is an ancient buried hill with gently sloping west-facing and steeply sloping north-facing inclines. The northeastern part of the bulge is a gradually rising slope (Fig. 1b), the east and west sides are controlled by boundary faults (Fig. 1c), and Cenozoic strata are deposited on both sides of the bulge. The exploration area is approximately 240 km^2, and the top buried depth of the Archean bedrock is < 4000 m. The Archean lithology is dominated by granite and granite gneiss. Because of the influence of the Indosinian, Yanshan and Himalayan tectonic movements, the Archean basement reservoirs in the Binxian area are mainly fractured reservoirs produced by tectonic processes and porous reservoirs formed by weathering and leaching. This forms a composite oilfield of the Archean bedrock buried hill and tertiary core-stratigraphic oil reservoir.

As a Cenozoic faulted basin, the Dongying Sag in Bohai Bay is under the thick Palaeogene and Neogene strata, storing most of the oil and gas. The Kongdian, Shahejie, Dongying, Guantao and Minghuazhen formations were mainly developed during the Cenozoic Era. However, the Archean granitic bedrock and the Cenozoic strata present an angular unconformity contact (Fig. 1d). The main source rock in this area is the widely developed thick Shahejie Formation, which directly covers the Archean weathering crust and provides sufficient oil and gas sources for the Archean weathered granite reservoirs in this area. The study of the weathered granite reservoirs therefore has important exploration significance.

3. Data and methods

3.a. Classification of lithological features and logging data

Under the influence of climate, topography, biology and other factors, the hard-textured granite is subjected to different intensities of weathering, forming a highly heterogeneous weathering crust with evident vertical zoning characteristics (Yang, 2004; Deng & Peng 2009; Li *et al.* 2011*b*; Lu *et al.* 2012). An overall core identification of the granite weathering crust was conducted, and the structural type of the crystalline rock, the proportion of granite blocks, and the difference in the colour and degree of fracture development were analysed. A scanning electron microscopy analysis of the different types of cores was conducted to analyse the proportion of main minerals and the type of pore structure. Finally, through the analysis of the above characteristics, the Archean weathered granite reservoirs in the Binxian area could be divided into three types: regolith, dissolution and fracture zones. The logging curves most sensitive to the three types of weathered granite reservoirs were acoustic (AC), density (DEN), natural gamma ray (GR) and resistivity (Rt) logging. These values were obtained by borehole compensated acoustic log, compensated density log, gamma ray log and dual laterolog log, respectively, with vertical resolutions of 5, 46, 30 and 51 cm. After normalizing the four types of logging curves, the data differences between the three different types of weathered granite reservoirs were

https://doi.org/10.1017/S001675682200053X Published online by Cambridge University Press

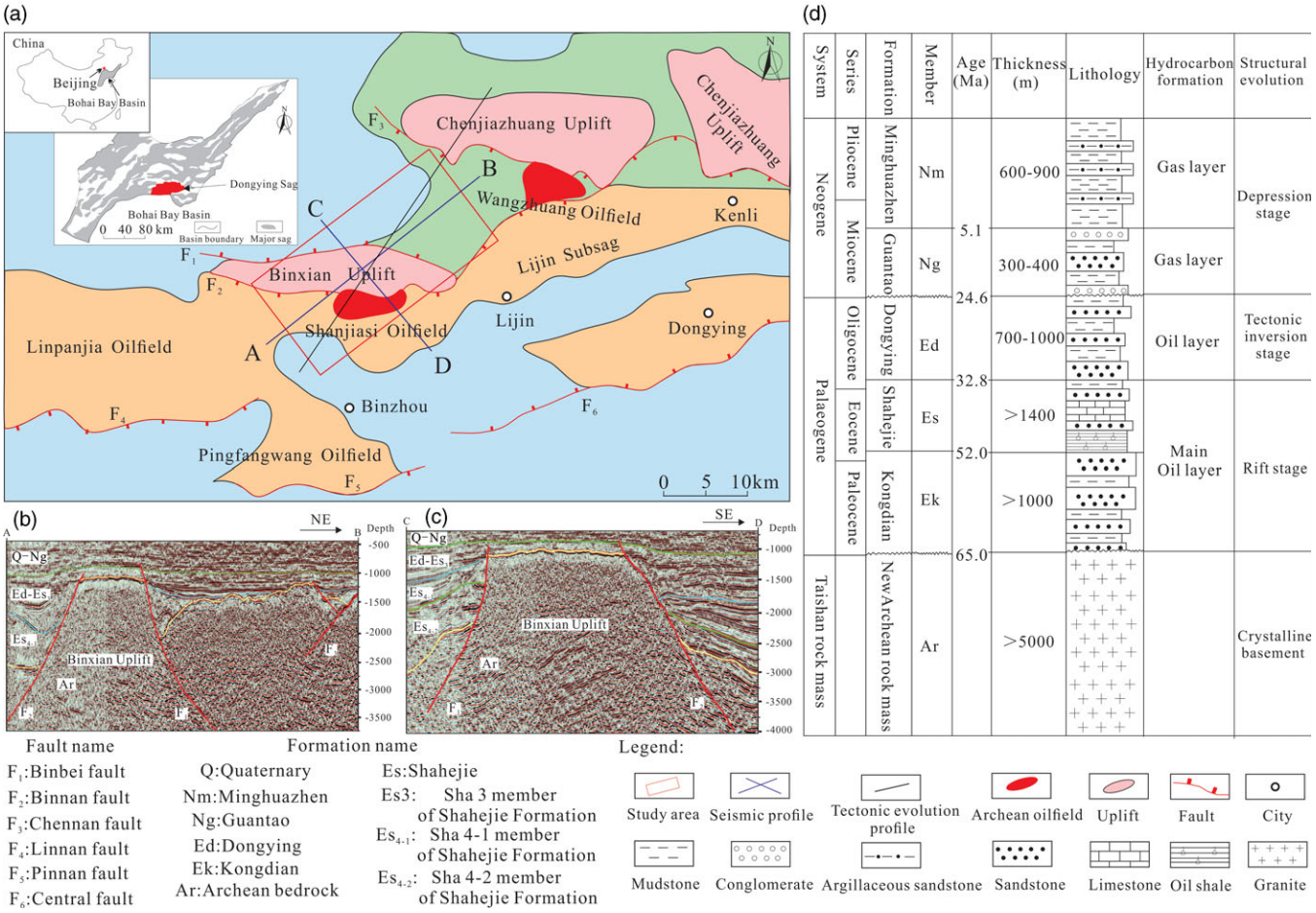

Fig. 1. (Colour online) (a) Structural location map of Binxian Uplift and the location of Archean granite oil reservoirs in the adjacent area. (b) NE seismic section (section A–B); the Archean stratum in the study area is an uplift controlled by faults on both sides, and the NE direction of the Binxian Uplift can be characterized by a gradually rising slope. (c) SE seismic section of the study area, where both sides of the main body of the Binxian Uplift are covered by thick Cenozoic strata that are in an angular unconformity contact with the Archean bedrock (software: Kingdom v. 8.8). (d) Lithostratigraphy and tectonic history of the Binxian Uplift (modified from Ji, 2015).

analysed, and logging response standards for the regolith, dissolution and fracture zones were established.

3.b. Calculating the physical properties of the reservoir using the dual-porosity-medium model

As a highly heterogeneous weathered granite reservoir because of leaching, dissolution and late structural transformation, the difference in the degree of fracture development makes it a typical multi-porous medium model (Zhang *et al.* 2008; Chen *et al.* 2010; Haskell *et al.* 2010; Zhu *et al.* 2018). Determining the physical properties of the reservoir is different from determining the physical properties of conventional sedimentary rocks. Adopting a suitable method for calculating the physical properties of the reservoir is essential for evaluating Archean reservoirs in the study area. The calculation method based on the matrix and fracture dual media is the most accurate and reasonable for the reservoir physical properties (Gu *et al.* 2008; Zhang *et al.* 2008; Zhang, 2010; Ma *et al.* 2017; Zhu *et al.* 2018). In this method, the storage space of the reservoir is divided into two parts: matrix and fracture. The sum of the matrix porosity (Φ_b) and fracture porosity (Φ_f) is the total porosity (Φ), and the total permeability (K) is the sum of the matrix permeability (K_b) and fracture permeability (K_f).

The matrix porosity was calculated using the multiple regression fitting method. The curve-fitting analysis results showed that the three types of porosity logging parameters were more sensitive to the granite porosity response. The acoustic (AC), density (DEN) and neutron logging (CNL) correlation coefficients – 0.6751, 0.7568 and 0.6654, respectively – were selected as the control variables for the matrix porosity multivariate fitting model; these porosity-logging tools are the most useful conventional logs for defining fractured zones (Cuong & Warren, 2009). The correlation coefficient between the matrix porosity calculated using the multivariate fitting method and the measured core porosity is 0.8279 (Fig. 2a).

The fracture porosity parameters were obtained by formation microscanner imaging (FMI) logging (Delhomme, 1992; Parra *et al.* 2009; Xu *et al.* 2021). The fracture width was calculated using the finite element method of Schlumberger's Geoframe software. Its principle is that diverse fracture widths can lead to various areas of conductivity anomalies. The fracture width is estimated using an empirical formula between the high-conductivity anomaly area and the resistivity of the formation and mud, and the fracture length is the sum of the fracture lengths on the borehole wall per unit area (Zhu *et al.* 2018). The correlation coefficient between the calculated total porosity and the measured core porosity is

https://doi.org/10.1017/S001675682200053X Published online by Cambridge University Press

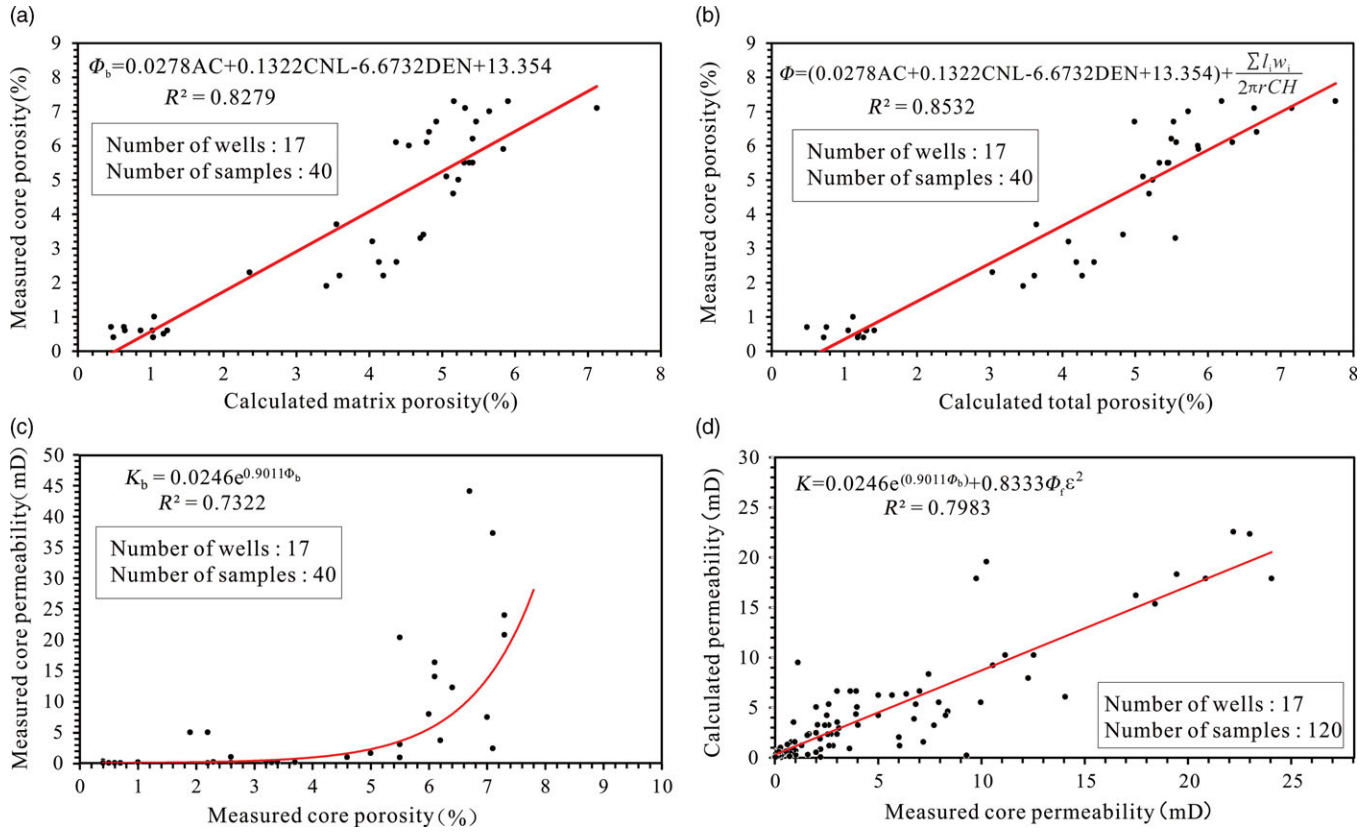

Fig. 2. (Colour online) Calculation and analysis diagram of the physical properties of weathered granite crust reservoir. (a) Validation analysis diagram of matrix porosity (calculated using the multivariate fitting method) and the measured matrix porosity. (b) Validation analysis diagram of total porosity (calculated using the dual-porosity-medium model method) and the measured porosity. (c) Fitting formula of the measured porosity of the core and the measured permeability of the core, establishing a calculation method for the matrix permeability of the weathered granite reservoir. (d) Validation analysis diagram of permeability (calculated using the dual-porosity-medium model method) and the measured permeability.

0.8532 (Fig. 2b). The total porosity of the weathered granite reservoirs can be calculated as follows:

$$\phi = \underbrace{(0.0278\ \mathrm{AC} + 0.1322\ \mathrm{CNL} - 6.6732\ \mathrm{DEN} + 13.354)}_{\phi_b} + \underbrace{\frac{\sum l_i W_i}{2\pi r\ C\ H}}_{\phi_f}$$

where Φ is the total porosity value (%); Φ_b is the matrix porosity (%); Φ_f is the fracture porosity (%); AC is the acoustic time difference logging value (μs m^{-1}); CNL is the neutron logging value (%); DEN is the density logging value (g cm^{-3}); l_i is the length of the ith fracture within a specific depth range (mm); W_i is the width of the ith fracture (mm); r is the borehole radius (m); C is the FMI borehole coverage density, which decreases with increasing borehole radius; and H is the calculated well length (m).

Because of the development of fractures in a weathered granite reservoir, the influence of fracture permeability should be considered when calculating its permeability. The total permeability is the sum of the fracture permeability and matrix permeability (Zhang *et al.* 2008; Yang, 2014; Ma *et al.* 2017). Constrained by the measured permeability of the core in the study area, the relationship between the matrix porosity and the matrix permeability was obtained by fitting analysis to calculate the matrix permeability (Fig. 2c). The fracture permeability was calculated from empirical formulae for the fracture porosity, fracture width and fracture permeability. The core-containing fractures were selected, and formulae for the measured fracture porosity and the measured fracture permeability were obtained by fitting the estimated fracture width under the microscope (Gu *et al.* 2008). The imaging logging of each well was then applied to obtain the fracture width data, and the fracture permeability of the reservoir in each well was calculated using the formula. From this, the permeability of the reservoir in different wells was calculated. The calculated permeability was found to be in good agreement with the measured permeability of the core (Fig. 2d). The permeability of the weathered granite reservoirs K is calculated as:

$$K = \underbrace{0.0246\ e^{0.9011\phi_b}}_{K_b} + \underbrace{0.8333\ \phi_f \varepsilon^2}_{K_f}$$

where K is the total permeability value (mD); Φ_b is the matrix porosity (%); Φ_f is the fracture porosity value (%); and ϵ is the fracture width (mm).

3.c. Distinguishing seismic reflection characteristics

The amplitude of the seismic data, the continuity of the reflection axis, height of the reflection frequency and the internal reflection structure can be used to distinguish the weathering crust zoning to a certain extent (Deng & Peng, 2009; Gong, 2010; Zhang & Liu, 2014; Li *et al.* 2015). For weathered granite reservoirs in areas with no wells or few wells in the working area, we can only rely on the accurate distinction of seismic data. Because of the different degrees of weathering, the seismic responses of the different zoning

https://doi.org/10.1017/S001675682200053X Published online by Cambridge University Press

structures of weathering crusts are significantly different. By compiling synthetic seismic records, and using logging and core data to comprehensively calibrate the seismic data, three types of seismic reflection characteristics corresponding to the weathering crust zoning types were established (Fig. 3).

3.d. Prediction of weathered granite reservoir distribution

Based on the multi-element classification standards for the three types of reservoirs, the weathering crust of the 47 wells in the working area was divided based on the reservoir structure. On this basis, the seismic reflection characteristics of the different types of weathered-crust reservoirs were extracted, and the seismic attribute characteristics of the Archean bedrock in the study area were analysed. Finally, combined with the analysis of logging and seismic data, the planar spatial distribution of the different types of weathered granite reservoirs were determined (Bawazer *et al.* 2018).

4. Results

4.a. Reservoir characteristics of weathering crusts

4.a.1. Core characteristics

By observing the core and identifying rock slices, we found that the Archean rock types in Binxian area are dominated by granite, followed by diorite and metamorphic rocks. Among them, granite is mainly grey-red and light flesh-red monzonitic, with a medium-grained and massive structure. Feldspar and quartz are the main mineral types, and there is intrusion of diorite bodies and pegmatite veins. Three different types of weathering crust structures are evident in the 47 coring sections, and can be divided into regolith, dissolution and fracture zones based on their characteristics.

The regolith presents an overall sandy soil structure; it is a deposit of weathered residual breccia and weathered clay, and the granite parent rock structure has disappeared (Fig. 4a). The plagioclase in the mineral has been weathered into scattered kaolinite, biotite has disappeared, quartz exhibits boundary erosion and intragranular dissolved pores are developed (Fig. 5a). The colour is grey or grey-green (Fig. 4b). Because of the long-term migration of oil and gas, some of the well bores appear as black sandy soil with a higher viscosity (Fig. 4c).

The dissolution zone is mainly composed of more than 70% of granite blocks and 10–30% of highly weathered cuttings and clay. The granite parent rock structure is relatively intact. The fractures in the granite present a network structure (Fig. 4c), with common intergranular pores. Feldspar dissolution pores can be seen (Fig. 5c), structural origin fractures dominate and a large number of joint fractures can also be seen (Fig. 5b). The reservoir space is dominated by pore–fracture type, followed by fracture type.

The fracture zone is mainly composed of granite rock blocks with a content of more than 90%. High-angle fractures can be seen (Fig. 4d). Occasionally, dolomite veins are filled in line. The fractures are different from those in the dissolution zone in that the high-angle and low-angle fractures intersect (Fig. 4e). The fracture density gradually decreases with increasing depth. Under an optical microscope, large intergranular gaps can be seen (Fig. 5e), multistage structural fractures are developed in a network shape (Fig. 5f) and the reservoir space is dominated by the pore–fracture type.

4.a.2. Log response characteristics

Based on the electrical survey response characteristics of the three types of reservoirs in the weathering crust, after making the logging data uniform across the working area, the differences between the logging data of various reservoirs were analysed. The weathering degree of the Archean weathered granite reservoirs was found to gradually weaken from the surface to the inside, that is, from the regolith to the dissolution zone to the fracture zone. The characteristics of the sonic log are gradually reduced. Density logging results show the opposite phenomenon, that is, a gradual increase in these characteristics. The resistivity decreases with increasing degree of weathering, and the neutron logging value gradually decreases with the weathering crust from top to bottom.

The logging response characteristics of the regolith were characterized using the high acoustic time difference (range: 7.91–23.39 μs cm^{-1}; average: 15.65 μs cm^{-1}), low density (range: 1.85–2.7 g cm^{-3}; average: 2.27 g cm^{-3}), high gamma value (range: 6–239 API; average: 122.5 API) and low resistivity (range: 1.98–30.48 Ω m; average: 16.23 Ω m). The log response characteristics of the dissolution zone were characterized by medium acoustic time difference (range: 5.05–16.44 μs cm^{-1}; average 10.75 μs cm^{-1}), medium to high density (range: 1.8–2.82 g cm^{-3}; average: 2.31 g cm^{-3}), medium to low gamma value (range: 8.5–120 API; average: 64.25 API) and medium resistivity (range: 12.37–91.85 Ω m; average: 52.11 Ω m). The logging response characteristics of the fracture zone are characterized by low acoustic time difference (range: 5.47–13.55 μs cm^{-1}; average: 9.52 μs cm^{-1}), high density (range: 2.4–2.96 g cm^{-3}; average: 2.68 g cm^{-3}), low gamma value (range: 2.2–118 API; average: 60.1 API) and high resistivity (range: 63.25–379.59 Ω m; average: 221.42 Ω m) (Table 1).

4.a.3. Petrophysical characteristics

The calculated physical properties of the different reservoirs across the entire area showed that those of the weathered granite reservoirs are highly variable vertically. Because of the inconspicuous granite parent rock structure of the regolith and the nature of the sandy gravel deposits, the fractures in the reservoir are not developed; however, the pores are developed. For example, the typical residual layer in Well S30 in the working area has a porosity range of 6–8% and a permeability range of 0.7–5 mD. The porosity range of the residual layer in Well S126 is 4–6%, and the permeability distribution range is 0.85–6.2 mD. The dissolution zone has superior physical properties; the reservoir space is more developed with pores and fractures, and its physical properties are better than those of the residual and disintegrating layers. For example, the dissolution zone of Well SG6 has a porosity range of 3–6% and a permeability range of 0.3–5.53 mD. The physical properties of the fracture zone are poorer than those of the dissolution and residual layers, and the porosity is low. Because the degree of weathering is not high, the rock is dense and the permeability is not high. For example, the median porosity of the fracture zone in Well S44 is 2–3%, and the permeability range is 0.01–0.7 mD. However, the development of fractures in local intervals improves the physical properties of the reservoir. For example, in Well SG6, the FMI image shows that there are fractured intervals, and the fracture porosity or permeability has a greater contribution to the total porosity or total permeability (Fig. 6a).

Through the calculation and analysis of weathered granite reservoirs in the 17 wells in Binxian Uplift, it can be concluded that the porosity range of the regolith is 5–9%, the porosity range of the dissolution zone is 2–7% and the porosity range of the fracture zone is 1–4% (Fig. 6b). The permeability ranges of the regolith, dissolution and fracture zones are 0.7–10, 0.1–5 and 0.01–0.5 mD, respectively (Fig. 6c). The three types of weathering crusts were compared and analysed. The regolith is a high-porosity and

https://doi.org/10.1017/S001675682200053X Published online by Cambridge University Press

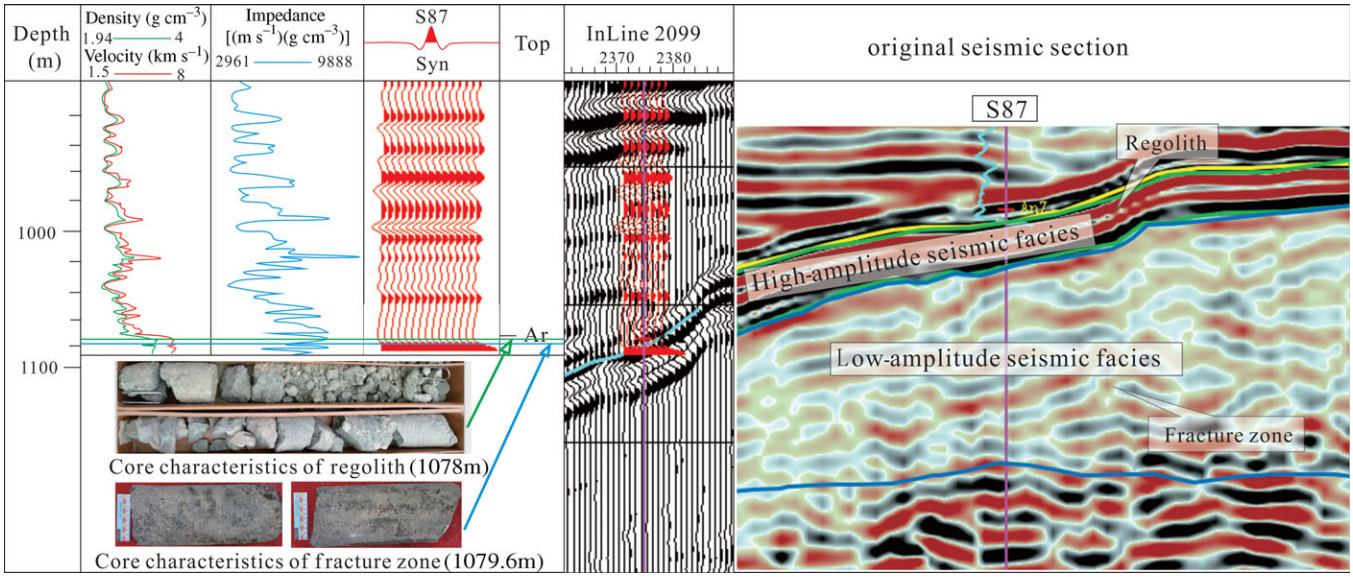

Fig. 3. (Colour online) Core depth calibration and synthetic seismic record calibration map, produced by synthetic seismic records, obtained by accurately combining core observations, logging data and seismic response characteristics; the seismic reflection characteristics corresponding to the different weathered granite reservoir structures can be identified.

Fig. 4. (Colour online) Images of different weathered granite reservoir cores taken from wells. (a) Regolith, greyish white, gritty, weathered granite, original structure destroyed by weathering (Well S87, 1070–1080 m). (b) Regolith, dark-grey massive coarse-grained granite with traces of weathered remains (Well S6, 1078.2 m). (c) Regolith, remaining oil spots (Well LGX601, 3094 m). (d) Dissolution zone, flesh-red quartz feldspar sandstone, development of articular cracks and dissolved pores (Well Z362, 1219.4 m). (e) Fracture zone, greyish-white medium-grained granite, two groups of cracks with different angles (Well S18, 1185 m). (f) Fracture zone, grey blocky granite and reticulated multiple groups of cracks (Well S133, 1384.6 m).

medium-permeability reservoir, the dissolution zone is a medium-porosity and medium-permeability reservoir, and the fracture zone is a low-porosity and low-permeability reservoir. However, there are abnormally high-porosity and high-permeability layers in the dissolution and fracture zones; these are closely related to fracture development.

4.a.4. Seismic response characteristics

Through the core-logging seismic calibration of different weathered granite reservoirs, it can be observed that the regolith exhibits a high-amplitude seismic profile and the seismic reflection event axis has good continuity. This is consistent with the high degree of weathering residual layer, stratified with the overlying deposits. The medium amplitude corresponds to the dissolution zone although it shows layered reflection in the lateral direction, but the continuity is not strong. The event axis presents a narrow range of twists in the same direction, with parallel and sub-parallel reflection characteristics. Compared with the strong amplitude, the amplitude intensity is evidently weakened. The low-amplitude seismic profile corresponds to the fracture zone; the internal reflection interface is messy, the event axis is unclear, the extension is the lowest, and the reflection frequency is the lowest compared with the medium- and high-amplitude seismic profiles. The section shows blank and messy reflection characteristics; occasionally,

https://doi.org/10.1017/S001675682200053X Published online by Cambridge University Press

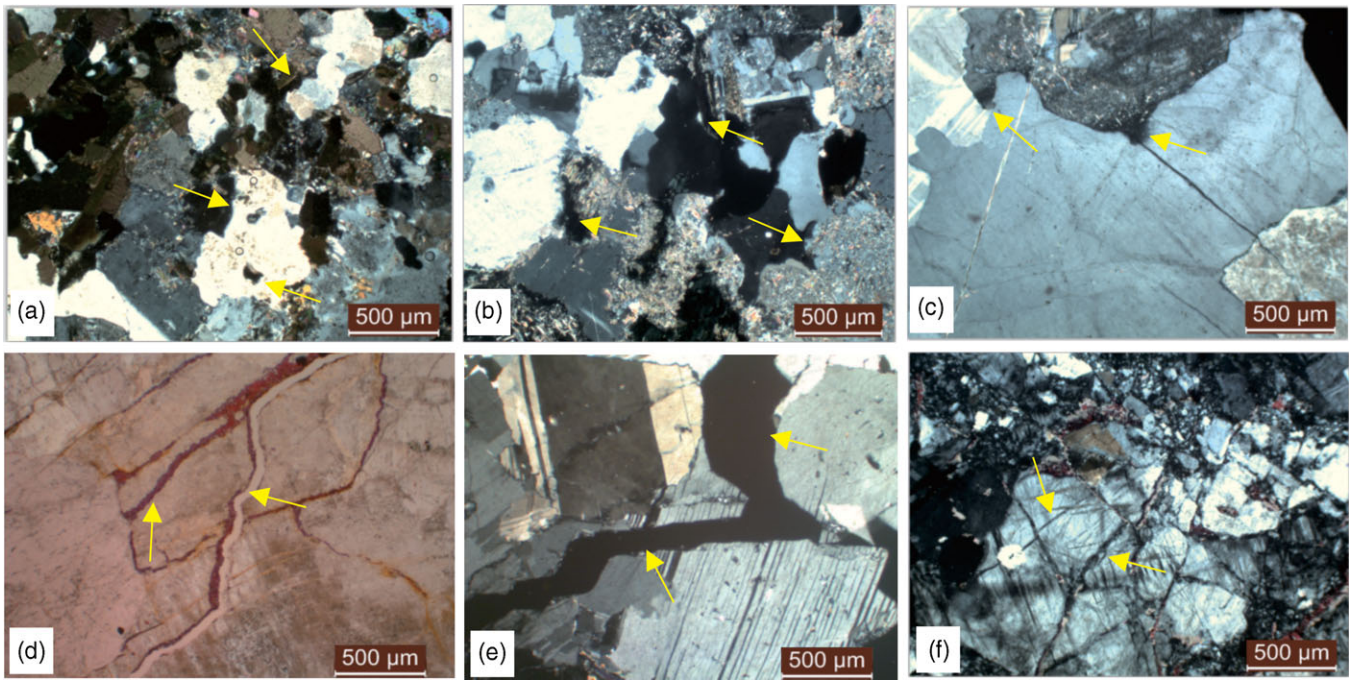

Fig. 5. (Colour online) Photomicrographs illustrating the mineral composition and main pore types within the weathered granite reservoirs. (a) Quartz is corroded and presents granular solution pores (Well Z366, 1330 m). (b) Intergranular pore (Well Z10, 1563.6 m). (c) Feldspar is corroded to form intergranular pores (Well Z4, 1590 m). (d) Structural crack, joint fissures (Well Z15, 1923.99 m). (e) Intergranular cracks can be seen in potash feldspar (Well Z13, 1761.03 m). (f) Multistage structural fractures show a network development (Well Z415, 1888.6 m).

the high-angle reflection event axis is interspersed. This is consistent with the low degree of weathering of the fracture zone and the development of high-angle cracks, which generally approach the chaotic reflection characteristics of the granite itself (Fig. 7).

4.b. Vertical combination type and genetic model of weathering crust

4.b.1. Features of double-layer structure of weathered shell

Based on the characteristics of the above-mentioned different types of reservoirs, a multifactor classification standard was established and a double-layer structure model of the weathering crust was proposed. The complete vertical structure of the weathering crust was divided into a completely weathered layer (regolith–dissolution zone) and a semi-weathered layer (fracture zone) from top to bottom (Zhu *et al.* 2020).

The completely weathered layer is located on the top of the double-layer weathered shell structure. Based on the different degrees of weathering, the completely weathered layer is divided into regolith and dissolution zone. The regolith is composed of residual sand, gravel and clay from weathering. The resistivity curve is relatively flat in the regolith and gradually increases from the top to the bottom. The acoustic wave and resistivity curves show small fluctuations. The physical properties are relative to those in the dissolution zone, with higher porosity and permeability. The seismic characteristics correspond to the high-amplitude phase reflection characteristics. The degree of weathering of the dissolution zone is relatively low, and the dissolution pores, fractures and joints are developed. From top to bottom, the resistivity curve gradually increases to the maximum value, the acoustic curve gradually decreases and the physical properties are better than those in the fracture zone. The seismic profile corresponds to the medium-amplitude phase reflection characteristics.

Located below the regolith–dissolution zone, the semi-weathered layer is a fracture zone with a weak degree of weathering, and the original structure of the bedrock is preserved. This zone is mainly composed of granite blocks. The unique feature of this zone is that the fractures are quite developed and of multiple types; multi-stage fractures intersect. From top to bottom, the resistivity curve gradually increases to the maximum value, and the acoustic jet lag curve gradually decreases. The poor physical properties of this zone are significantly improved because of the development of fractures at some depths. This zone corresponds to the low-amplitude reflection characteristics on the seismic profile (Fig. 7).

4.b.2. Combination of vertical zoning and reservoir typing

The weathering crust in the working area has different vertical development characteristics in the different parts of the buried hill. Three types of vertical stacking weathering crust combinations are developed in the working area. Type I is the regolith covering the fracture zone; type II is the dissolution zone covering the fracture zone; and type III is the separate development of the fracture zone (Fig. 8).

Different types of weathering crusts evolve gradually. First, the vertical structure of the weathering crusts in the study area varies with the change in the structural positions. Second, the regolith and the dissolution zone do not develop at the same well. For example, the fracture zone is directly developed at the top of Well Z39. There is a dissolution zone at the top of Well Z362, and no regolith is seen. The regolith is developed at the top of Well Z366 (Fig. 9). The evolution process of the granite weathering crust is as follows: the fracture zone is further weathered to form a dissolution zone with developed dissolution pores, and the final product formed in the later stage of weathering is the regolith. If weathering continues, the regolith will be eroded, the fracture zone will be exposed and the next stage of weathering cycle will begin; the top of the weathering crust structure therefore changes. With different

https://doi.org/10.1017/S001675682200053X Published online by Cambridge University Press

Table 1. Log response characteristics of different granite weathered-crust reservoirs from 47 wells in the study area

	Acoustic (AC, μs cm^{-1})		Density (DEN, g cm^{-3})		Gamma ray (GR, API)		Resistivity (Rt, Ω m)	
Weathering crust	Min, max	Ave	Min, max	Ave	Min, max	Ave	Min, max	Ave
Regolith	7.91, 23.39	15.65	1.85, 2.7	2.27	6, 239	122.5	1.98, 30.48	16.23
Dissolution zone	5.05, 16.44	10.75	1.8, 2.82	2.31	8.5, 120	64.25	12.37, 91.85	52.11
Fracture zone	5.47, 13.55	9.52	2.4, 2.96	2.68	2.2,118	60.1	63.25, 379.59	221.42

Note: Minimum value–maximum value/average value, the data come from 47 wells in the study area.

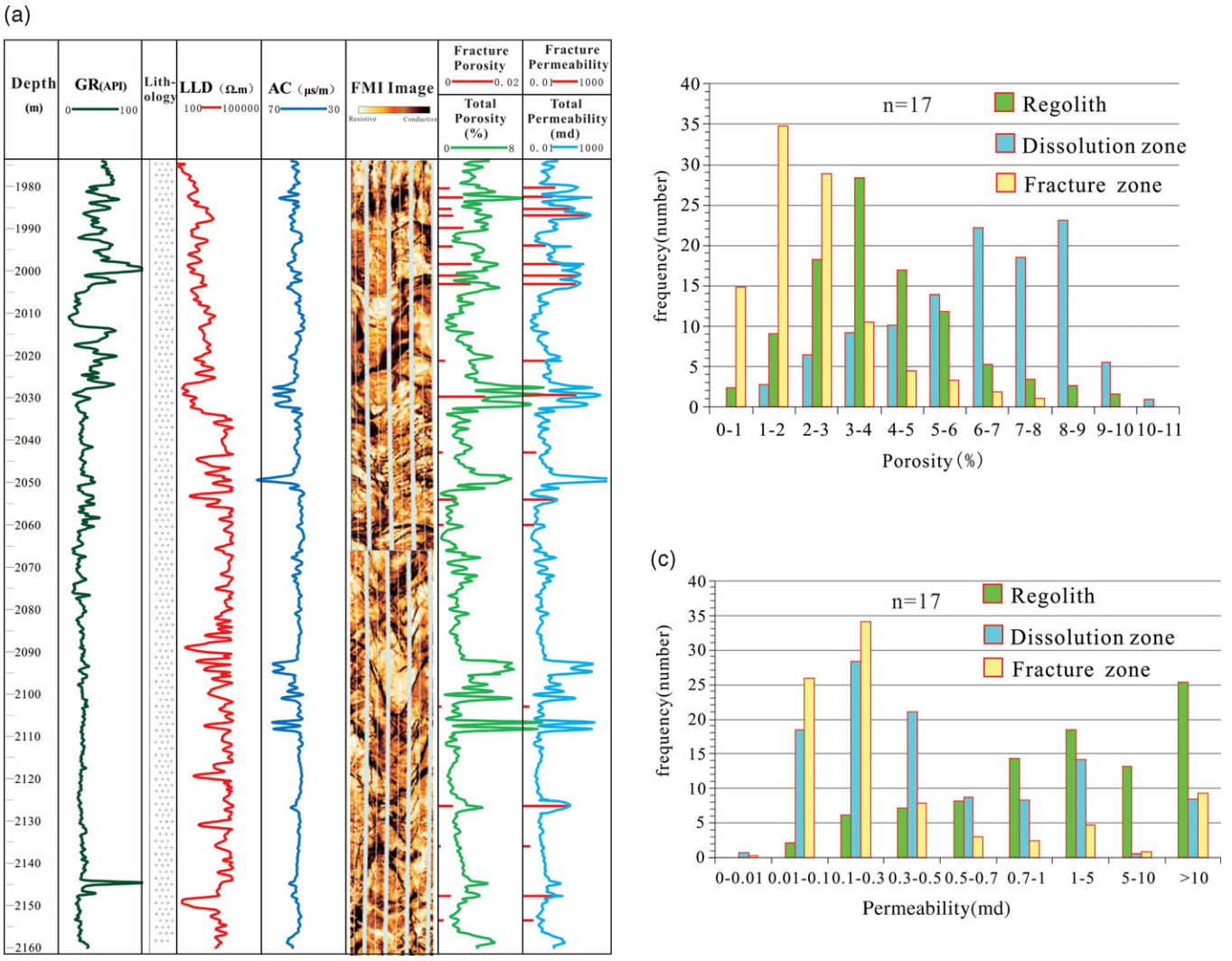

Fig. 6. (Colour online) Analysis map of the physical properties of the weathered granite reservoir in the study area. (a) Logs of weathered granite reservoirs at a measured depth (MD) of 1970–2160 m in Well SG6 of Binxian Uplift. FMI logging is used to obtain the fracture data and then calculate the fracture porosity and fracture permeability (red rod-shaped). (b) Distribution frequency histogram of the porosity of different weathered granite reservoirs. (c) Permeability distribution frequency histogram of different weathered granite crust reservoirs. GR – gamma ray; LLD – resistivity log; AC – sonic log; FMI – fullbore formation microimager log.

evolution stages, the vertical zoning of the granite weathering crust reservoir varies.

4.c. Distribution characteristics of weathered granite reservoirs

4.c.1. Vertical distribution

By classifying the structure of the 127 wells (according to core observations, logging data, physical properties and seismic reflection characteristics) drilled through the Archean granite weathering crust in the working area, it was found that the development of reservoirs of weathered granite types is different at different locations. The reservoir thickness varies significantly, which is closely related to the structural position of the well site and the degree of fracture modification in the subsequent period. Through the analysis of the weathered-crust structure of the wells at different locations (Fig. 10c), several important characteristics of the weathered granite reservoir distribution were obtained.

https://doi.org/10.1017/S001675682200053X Published online by Cambridge University Press

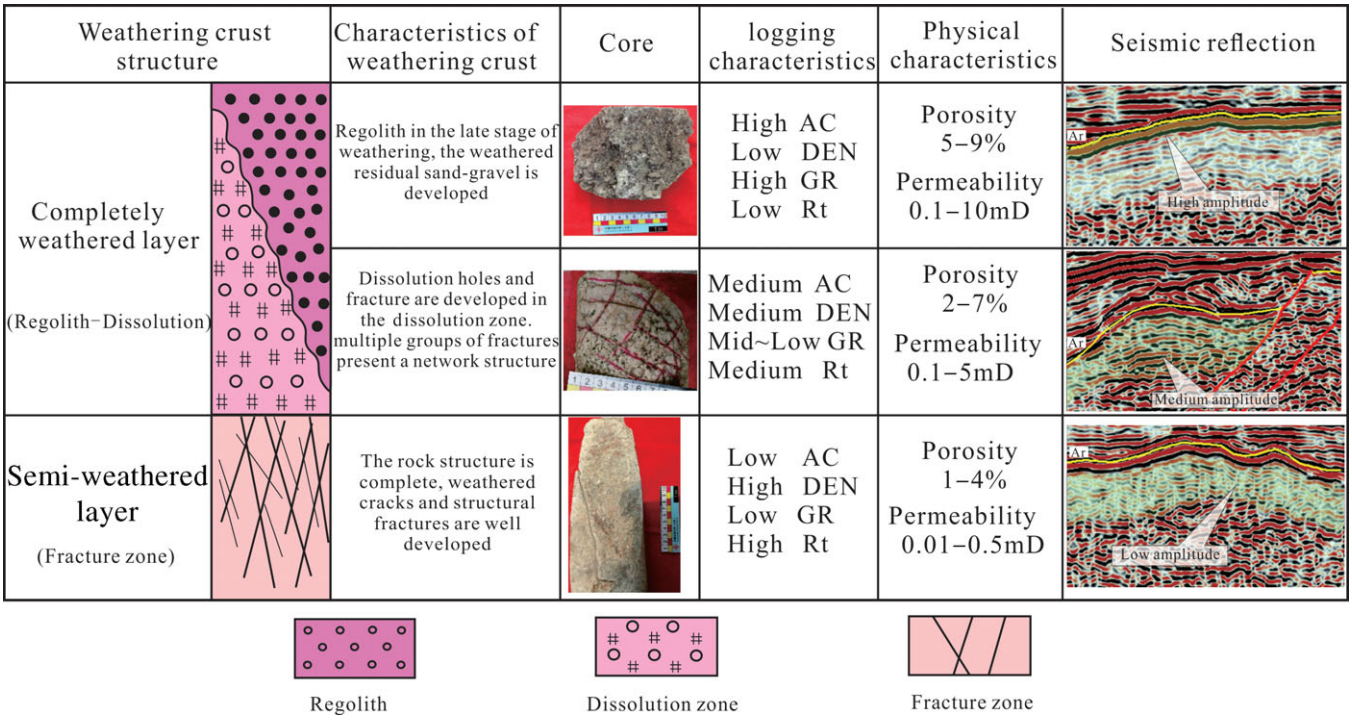

Fig. 7. (Colour online) Based on core observations, logging data, physical properties and seismic response characteristics, a classification standard is established for the double-layer structure of the Archean weathered granite reservoir in the Binxian Uplift. The complete reservoir structure is divided into an upper completely weathered layer and a lower semi-weathered layer. The completely weathered layer is divided into regolith and dissolution zone based on the evolution stage. The semi-weathered layer is the fracture zone.

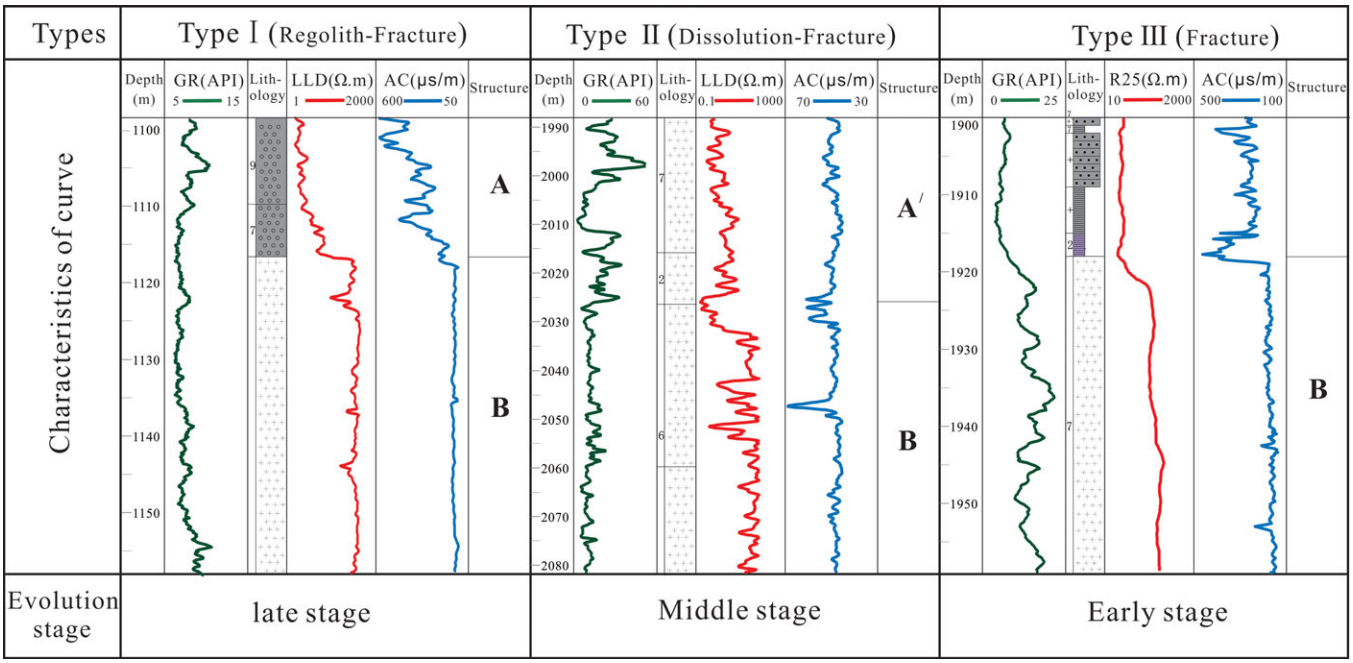

Fig. 8. (Colour online) Vertically superimposed types of weathered granite reservoirs in the Binxian Uplift. The vertical structure of the reservoirs is divided into three types: type I is the regolith covering the fracture zone; type II is the dissolution zone covering the fracture zone; and type III is the separate development of the fracture zone. A – regolith; A/ – dissolution zone; B – fracture zone.

The development of regolith is found in the gentle slope area of the bulge edge. Wells with more developed regolith in the working area are mostly distributed in the gently inclined slopes around the bulge and have good lateral continuity. The development position of the regolith can be intuitively reflected through the connected well profile in the uplift and gently inclined slope areas (Fig. 10a). The dissolution zone is developed in the lower part of the structure. The fracture zone of the high part of the structure

https://doi.org/10.1017/S001675682200053X Published online by Cambridge University Press

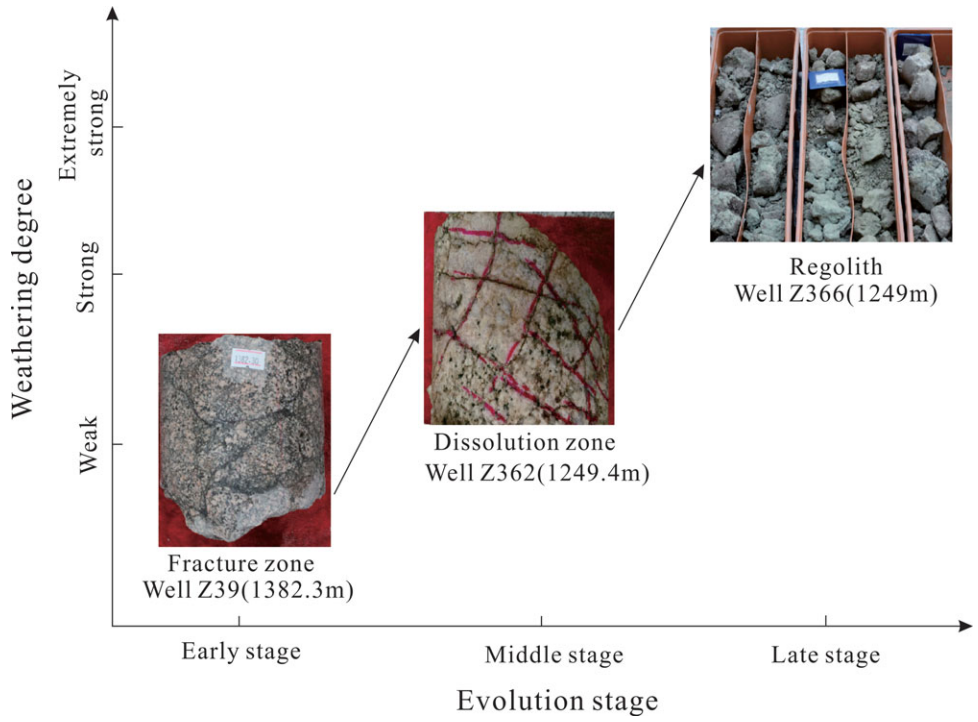

Fig. 9. (Colour online) Schematic of the weathering degree and evolution stage of the top structure of the weathered granite reservoir in Binxian Uplift. In the core of the borehole, the fracture zone with a complete parent rock structure is developed on top of the Archean strata in Well Z39, a dissolution zone with pores and fractures is developed on top of the Archean bedrock in Well Z362 and a gritty regolith is developed in Well Z366.

is exposed, and other parts are covered under the regolith or the dissolution zone. The connected well profile inside the working area reveals that there is a thick fracture zone in the high part of the granite buried hill structure (Fig. 10b).

4.c.2. Planar distribution

To analyse the planar distribution of granite, previous authors have tried using instantaneous phase properties, energy properties and numerical simulation methods (Wang *et al.* 2003; Li *et al.* 2009; Zhu, 2012; Li *et al.* 2016; Zhang & Chen, 2017). The maximum-amplitude attribute along the layer was used to extract the seismic reflection amplitude of the weathered granite reservoirs for confirmation. First, a time window of 30 ms was set on the top surface of the Archean bedrock. The maximum amplitude attribute map shows that the high-amplitude distribution limit is mainly distributed in the gently inclined slope area near the structural high point (Fig. 11a). Subsequently, to eliminate the influence of high reflection at the top, the extraction time window was adjusted to a range of 75–120 ms. At this time, the maximum attribute map has mainly two reflection characteristics of medium and low amplitudes. The medium amplitude is distributed in the low part of the slope, and the low amplitude is distributed in the high point of the buried hill structure and the low part of the southern part of the work area (Fig. 11b). The distribution has evident characteristics of ring-shaped extension, and the extracted amplitude attribute map shows that this feature is consistent with the seismic facies division feature and the logging division feature.

We identified the seismic facies corresponding to the weathering crust structure, and combined the logging data and core data to obtain the plane distribution map of the weathering crust structure (Fig. 12). Regolith is mainly distributed on the slope near the southern slope of the structural high point of Binxian Uplift; the dissolution zone is located below the regolith and is distributed at the foot of the southern slope of the Binxian Uplift. The dissolution zone distribution area in the other areas is located in the buried hill depression in the NE direction of the Binxian Uplift. The fracture zone develops in a wider range. A high point of the Binxian Uplift is developed adjacent to the Binnan Fault. The dissolution zone in the southern part of the work area also covers the development area of the fracture zone.

5. Discussion

5.a. Evaluation of oil-bearing reservoir

By clarifying the distribution of weathered granite reservoirs, it is important to conduct an oil-bearing evaluation of the reservoir. With the qualitative identification of oil layers, based on coring, oil testing and production test data, combined with drilling and logging data, we determined the lower limits of the physical properties of the oil-bearing reservoir. Based on the analysis of the measured physical properties of the oil-bearing cores of 13 wells in the working area, the lower limits of the porosity and permeability of the Archean weathered-crust oil-bearing reservoir in the Binxian area were found to be 1.8% and 0.1 mD, respectively (Fig. 13a). The oil stain in the regolith accounts for the highest proportion of its statistical thickness, reaching 52.3%. There is also a 1.3% oil immersion level display. The dissolution zone has high oil content overall, with an oil stain of 38.5% and an oil trace level of 6.8%. The fracture zone has the highest fluorescence display ratio, followed by an oil stain of 27.2% (Fig. 13b). In the comprehensive interpretation of the thickness statistics chart, the oil reservoir accounted for 13.2% of the regolith, the low-concentration oil layer accounted for 30.4% and the dry layer thickness was small. The oil layer accounted for 8.9% of its statistical thickness of the dissolution zone, and the low-concentration oil reservoir accounted for 28.3%. The fracture zones are mainly composed of water and dry layers, and the thickness of the oil-bearing reservoirs is relatively small (Fig. 13c). From the overall analysis, although the regolith is thinner its oil-bearing capacity is good. The dissolution zone is the reservoir with the most exploration potential, with a thicker

https://doi.org/10.1017/S001675682200053X Published online by Cambridge University Press

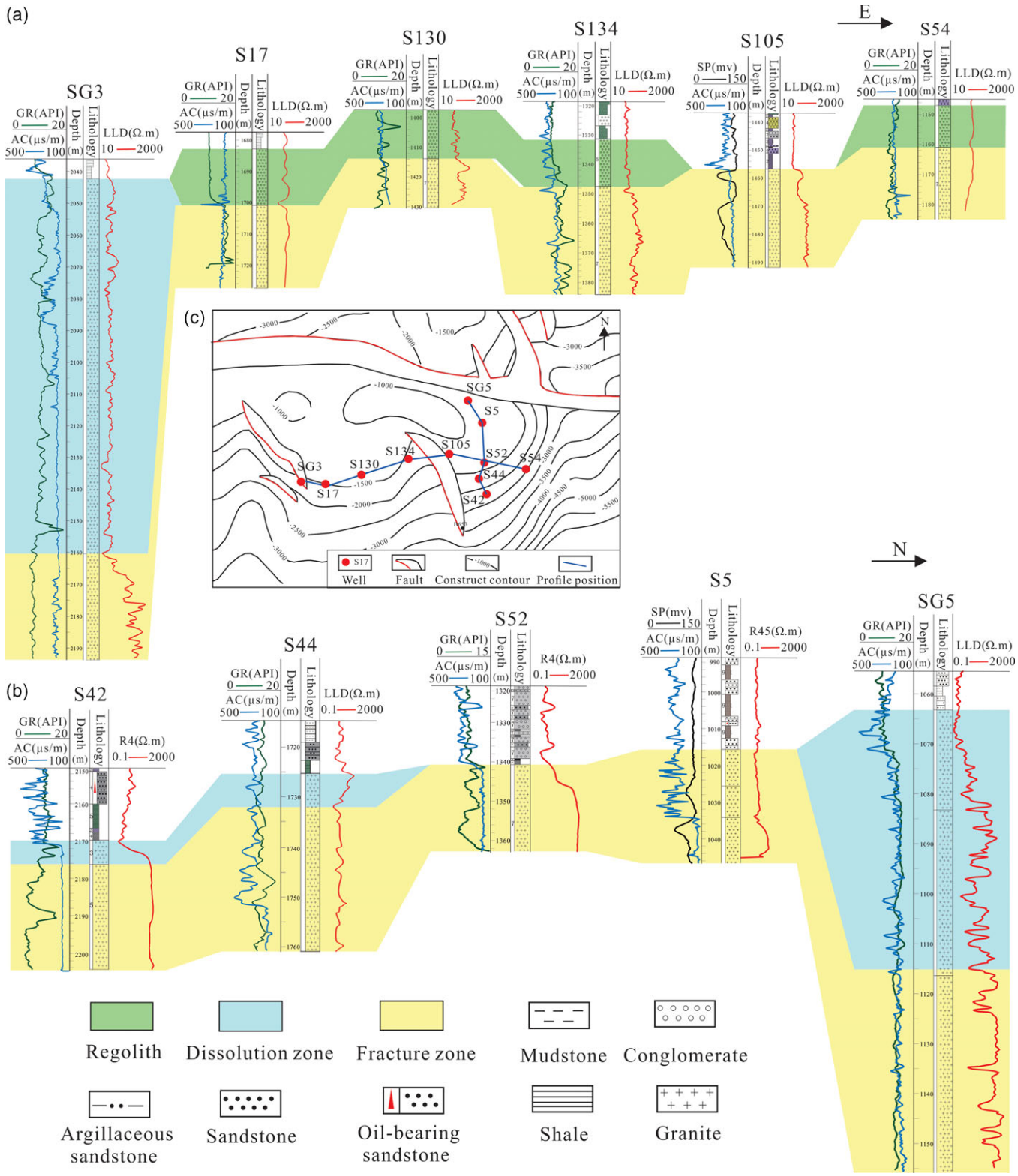

Fig. 10. (Colour online) Connected well profile of Archean bedrock in Binxian Uplift. Regolith is developed in the gently inclined slope zone adjacent to the structural high point with good lateral continuity; the dissolution zone is developed in the low structural part and is thicker; the fracture zone is exposed at the structural high point. (a) E–W-connecting well profile. (b) N–S-connecting well profile. (c) Schematic of profile location.

https://doi.org/10.1017/S001675682200053X Published online by Cambridge University Press

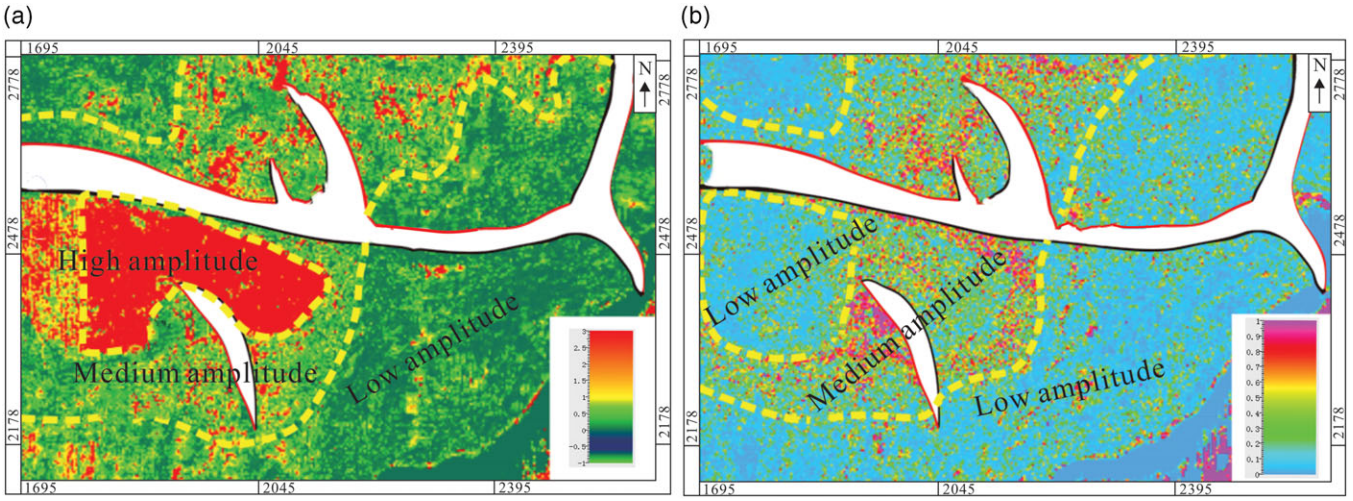

Fig. 11. (Colour online) Plane distribution map of the maximum amplitude attributes of seismic data in the Binxian Uplift. (a) Maximum amplitude attribute distribution diagram with a reflection time window of 30 ms from the top surface of the Archean Realm. (b) Maximum amplitude attribute distribution diagram with a time window of 75–120 ms, which eliminates the impact of seismic reflections resulting from sudden changes in the top lithology of the Archean strata.

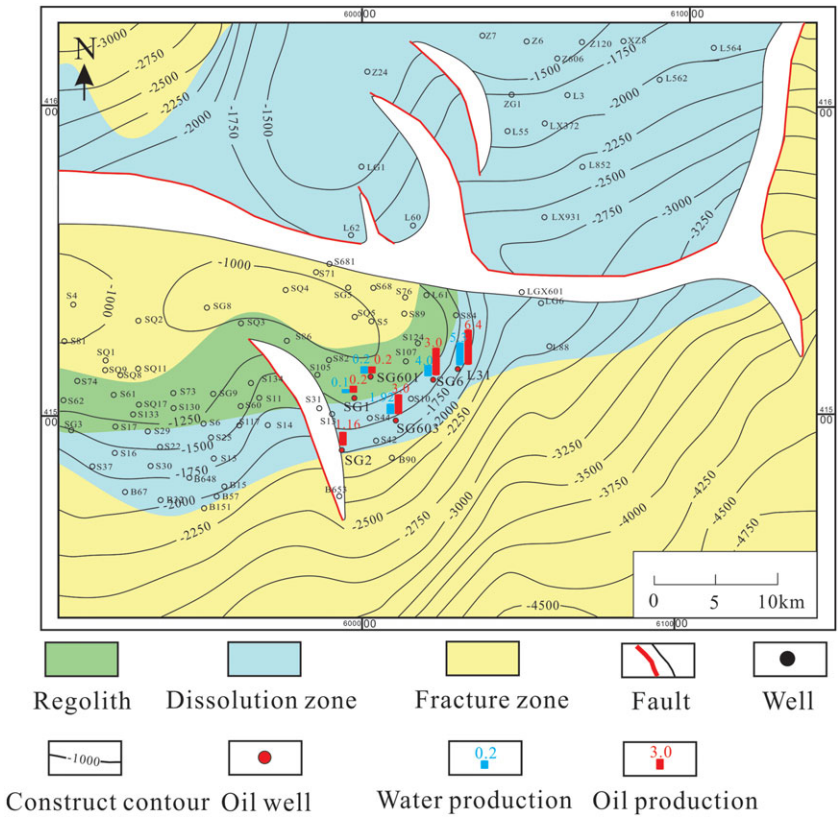

Fig. 12. (Colour online) Plane distribution map of Archean granite weathered-crust reservoir and oil-producing wells in Binxian Uplift. The fracture zone is developed in the entire area and exposed at the high point of the structure. Regolith and dissolution zone are developed in the slopes and low structural parts, which are the main oil-producing well distribution areas.

structure and relatively good oil-bearing capacity. The fracture zone has relatively poor oil-bearing properties, but its fractures are well developed and the thickness is large, meaning that it still has a certain exploration value.

By analysing the current data of the Archean weathered-crust oil production wells, it was found that the wells located in areas where the regolith and the dissolution zone are developed have higher oil production. In the regolith near the gently inclined slope of the structural high point, the daily oil production of Well SG601 was 0.2 t. Wells with high yields in the dissolution zone at the foot of the slope were discovered. The daily oil production of Well L34 was 6.4 t and that of Well SG6 was 3.0 t (Fig. 12). From the perspective of the location of the oil production wells and the oil content in the reservoir, the idea of structural high point exploration is inapplicable to weathered granite reservoirs in the study area. The regolith and dissolution zone are located on the slope; the foot of the slope has great exploration potential, providing new ideas for the exploration of weathered granite reservoirs.

https://doi.org/10.1017/S001675682200053X Published online by Cambridge University Press

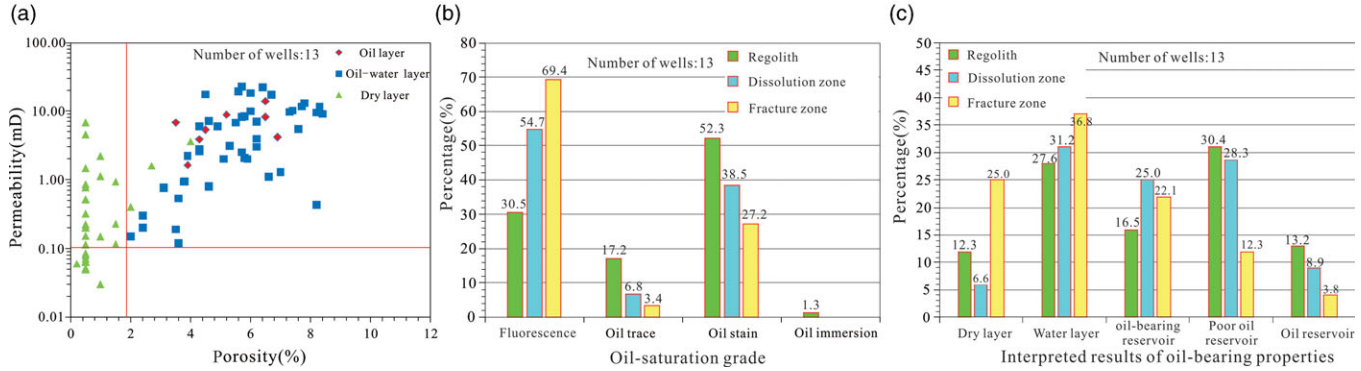

Fig. 13. (Colour online) Oil-bearing analysis map of Archean weathered granite reservoir in the Binxian Uplift. (a) Analysis of the lower limit of the oil-bearing physical properties of weathered granite reservoirs. (b) Statistical histograms of oil-saturation-grade thickness of different weathered granite reservoirs. (c) Statistical histogram of the interpretated thickness of different weathered granite reservoirs.

5.b. Rotation of the bedrock block causes weathering crust to tilt

The Bohai Bay Basin is a rift basin developed under the stress of two sets of faults cutting towards the NW and NE. The half-graben depression is the basic structure inside the basin, and is also the result of the continuous rotation of the bedrock fault block. This type of half-graben depression is also widely developed in the Dongying Sag, and the distribution of the weathering crust is also affected by the direction and angle of the tilt of the fault block (Lan, 1984; Yang *et al.* 2004; Liu & Wang, 2010). There are mainly three types of weathering-crust tilting patterns inside the working area: stepped fault block, reverse rotating block and positive rotating block. In the stepped fault block tilting model, the weathered crust slides down along the fault plane because of the instability at the edge of the fault. The section appears as a shovel-type normal fault that merges downwards (Fig. 14a). Under the action of the tensile stress in the tilting fault block, the bedrock block rotates along the fracture surface of the fault. Based on the combined relationship of the attitude of the fault and the dip of the weathering crust of the bedrock, it can be divided into two styles: reverse tilt and positive tilt (Lan, 1984; Liu *et al.* 1997). In the reverse tilting style, the fault block rotates in the opposite direction and the bedrock fault block sandwiched by the two faults gradually rises toward the extension of the footwall of the fault. The weathered crust of the bedrock close to the footwall of the fault is weakened (Fig. 14b). The positive tilt is the opposite of this: the bedrock fault block rotates positively, causing the bedrock fault block to extend obliquely to the lower wall, forming slopes with evident differences in the weathering degrees (Fig. 14c).

The fault activity in the Dongying Sag has evident N–S differences and has the characteristics of segmentation in the time of activity (Qi *et al.* 2003; Ma *et al.* 2005; Ye *et al.* 2006; Tang, 2008; Zhang *et al.* 2009, 2019; Wang *et al.* 2017). It not only controls the sedimentary evolution of the Binxian area, but also affects the uplift and erosion of the weathering crust and controls the formation and destruction of the weathering crust (Zhu *et al.* 2004; Hou *et al.* 2005; Li *et al.* 2011*a*; Zhang *et al.* 2014). The tilt of the fault block is controlled by the fault and changes gradually with the geological evolution period, making it important to analyse the tectonic evolution process. This not only affects the distribution of the weathered granite reservoirs, but also plays an important role in controlling the accumulation of oil and gas (Zong *et al.* 1999; Gao, 2014; Fan, 2019; Xie, 2019). Taking the NE-trending large section of Binxian area as a representative case, the tectonic evolution of the Binxian area can be mainly divided into four stages. First, before the sedimentation of the Es4-2 formation, the Archean top surface was relatively gently inclined and there was a gully in the NE of the Binbei Fault. At this time, the fault block had not yet been displaced (Fig. 15a). Subsequently, before the sedimentation of the Sha 3 member of Shahejie Formation, the top of the Binxian Uplift was still subjected to weathering and erosion, and its NE gully deepened (Fig. 15b). Next, at the end of the deposition of the Dongying Formation, with the development of faults the fault blocks did not descend in parallel under the NE and SW tensile stress fields in the Dongying area. Rather, they rotated and tilted, which increased the buried depth and tilt of the well developed weathering crust in the middle (Fig. 15c). Finally, the present-day structural framework of the Archean buried hills and slopes of Lijin fault depression in Binxian Uplift was formed (Fig. 15d). The positive tilting effect occurred during the deposition process of the F1 fault and the Lijin area showed a gradually rising oblique wave, which significantly affected the differential weathering and preservation pattern of the later weathering crust. As a result, on the current profile the weathered granite reservoir is still well developed inside the buried hill sag; to a certain extent, this affected and formed the structural high point fracture zone exposed in the Binxian Uplift and the characteristics of the regolith and dissolution zone in the slope zone that gradually uplifted in the NE direction.

5.c. Reservoir potential variation

Later burial is an important factor for the preservation of weathered granite reservoirs. An early or late burial time brings about differences in the preservation characteristics of weathering crusts. Generally, weathering crusts buried early retain their complete zoning structure and are relatively thick. Conversely, the later the burial, the poorer the preservation characteristics. The weathering crust in the raised slope zone inside the working area is covered by sedimentary layer C (Fig. 16) earlier than the high part of the protrusion, and the weathering crust is less damaged by weathering and erosion; the corroded layer is therefore retained. Sedimentary layer B (Fig. 16) is accumulated later, the weathering crust continues to undergo weathering and denudation, and the late-product regolith that formed the weathering crust remains. Because of the late burial of sedimentary layer C, the weathering crust of granite located in the high part of the Binxian Uplift was not completely covered; the weathering crust of the granite was therefore seriously damaged as a result of weathering. The

https://doi.org/10.1017/S001675682200053X Published online by Cambridge University Press

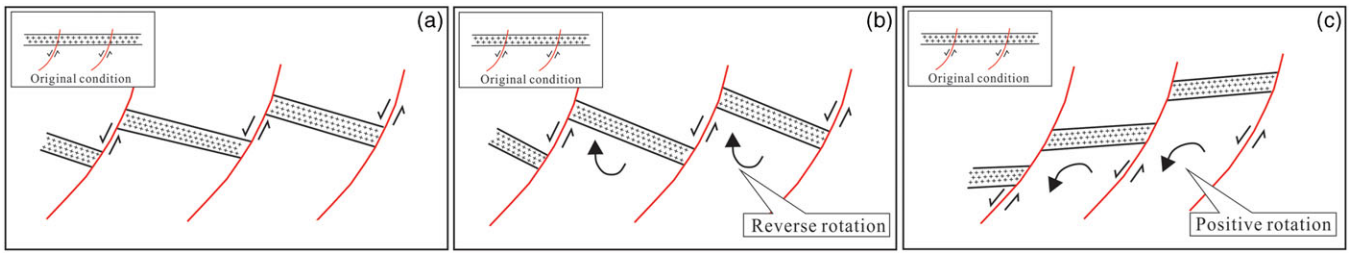

Fig. 14. (Colour online) Model diagram of fault block tilting type: (a) stepped fault block tilt; (b) fault block reverse tilt; and (c) fault block positive tilt.

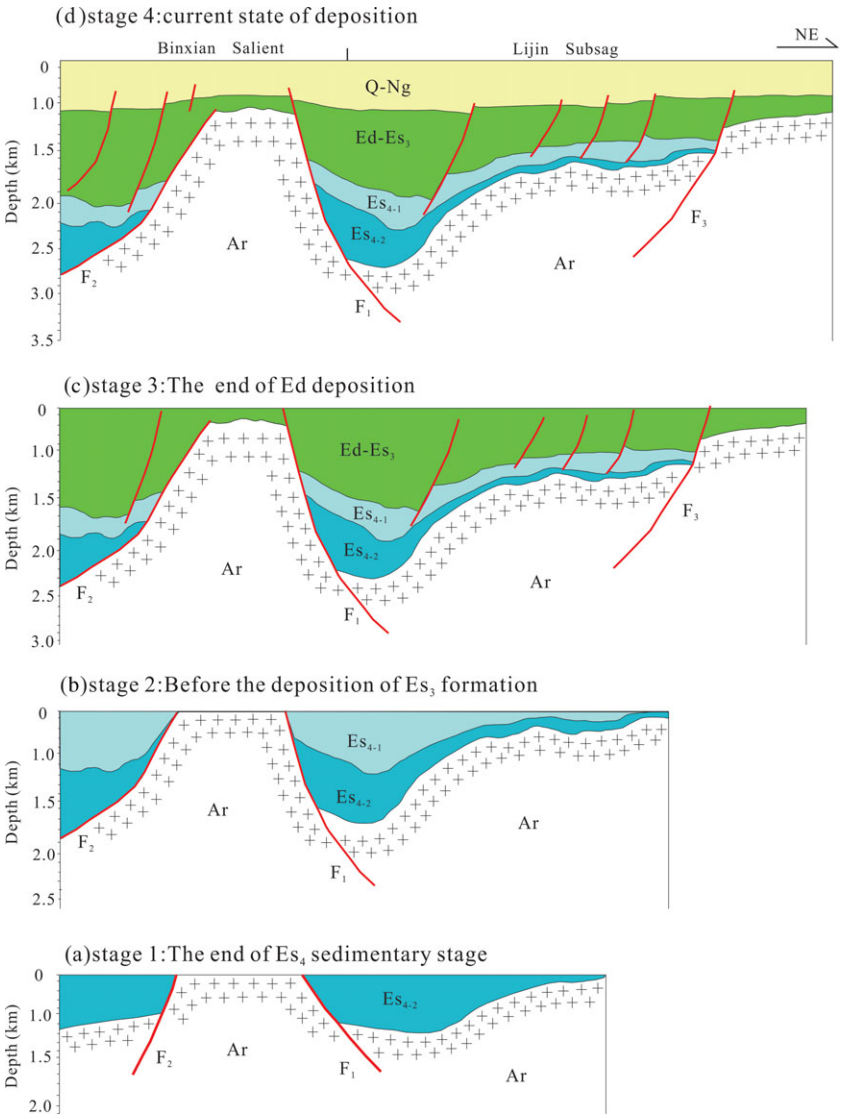

Fig. 15. (Colour online) Tectonic evolution history of Binxian salient. Q – Quaternary; Ng – Guantao Formation; Ed – Dongying Formation; Es3 – Sha 3 member of Shahejie Formation; Es4-1 – Sha 4-1 member of Shahejie Formation; Es4-2 – Sha 4-2 member of Shahejie Formation.

loose regolith and the dissolution zone of the upper layer were destroyed and eroded, although the fracture zone was maintained. The preservation degree and thickness of the weathered crust are therefore closely related to the burial time (Fig. 16).

6. Summary and conclusions

The Archean weathered granite reservoirs in the Binxian Uplift could be vertically divided into three zones: regolith, dissolution and fracture. The quantitative difference in the logging responses was found to be beneficial to the classification of reservoir types. Fractures significantly improved the physical properties of the weathered granite reservoirs. The regolith is a high-porosity and medium-permeability reservoir (porosity range: 5–9%; permeability range: 0.7–10 mD); the dissolution zone is a medium-porosity and medium-permeability reservoir (porosity range: 2–7%; permeability range: 0.1–5 mD); and the fracture zone is a low-porosity and low-permeability reservoir (porosity range: 1–4%; permeability range: 0.01–0.5 mD). In terms of the seismic response, the regolith corresponds to high-amplitude seismic facies, the dissolution

https://doi.org/10.1017/S001675682200053X Published online by Cambridge University Press

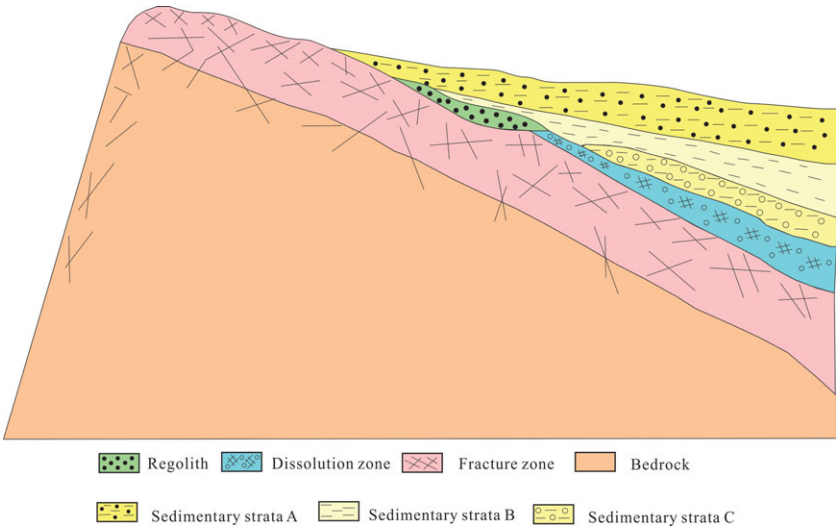

Fig. 16. (Colour online) Schematic of the difference in the preservation of weathered granite reservoirs. The burial time affects the difference in the preservation of weathered granite reservoirs. The weathered granite reservoir with an earlier burial time preserves the vertical zoning structure and has a relatively large thickness. Conversely, the later the burial, the poorer the preservation.

zone corresponds to medium-amplitude seismic facies and the fracture zone corresponds to low-amplitude seismic facies.

The regolith was distributed on a gently inclined slope near the structural high point, the dissolution layer was distributed at the foot of the slope and the fracture layer was exposed at the structural high point. With the change in the structural location, three types of vertically superimposed structures developed separately in the weathered granite reservoirs: regolith–fracture zone, dissolution–fracture zone and fracture zone. The regolith and dissolution zones presented better oil-bearing properties. In terms of their lower limits, the porosity and permeability of the weathered granite reservoir were 1.8% and 0.1 mD, respectively.

Based on differences between the core observations, logging data, physical properties and seismic response characteristics, the established multifactor identification criteria for reservoirs can help accurately identify different types of weathered granite reservoirs. The vertical structure varies with the structural position of the reservoir. At different structural positions, the reservoir has different overlapping relationships. The formation and preservation of granite weathering crusts is a geodynamic process, and the effects of fault block tilt and burial period of the overlying sedimentary layer on the formation, distribution and preservation of the reservoir should be considered. Favourable reservoirs (residual and dissolution layers) for exploration are distributed in the slopes and low structural parts, and the idea of structural high-point exploration is no longer applicable to granite buried-hill oil reservoirs. In the future, structural slopes should be considered the main exploration direction in similar oil reservoirs.

References

Alberto C, Giulio V, Giulia T and Marco A (2021) In-situ quantification of mechanical and permeability properties on outcrop analogues of offshore fractured and weathered crystalline basement: examples from the Rolvsnes granodiorite, Bømlo, Norway. *Marine and Petroleum Geology* 124, 104859. doi: https://doi.org/10.1016/j.marpetgeo.2020.104859.

Armitage PJ, Faulkner DR and Worden RH (2013) Caprock corrosion. *Nature Geoscience* **6**, 79–80. doi: https://doi.org/10.1038/ngeo1716.

Bawazer W, Lashin A and Kinawy MM (2018) Characterization of a fractured basement reservoir using high-resolution 3D seismic and logging datasets: a case study of the Sab'atayn Basin, Yemen. *PLoS ONE* **13**, e0206079.

Belaidi A, Bonter AD, Slightam C and Trice RC (2018) The Lancaster field: progress in opening the UK's fractured basement play. In *Petroleum Geology of NW Europe: 50 years of Learning* (eds M Bowman and B Levell), pp. 385–98. Geological Society of London. Proceedings of the 8th Petroleum Geology Conference, 26 September 2016.

Bonter DA and Trice R (2019) An integrated approach for fractured basement characterization: the Lancaster Field, a case study in the UK. *Petroleum Geoscience* **25**, 400–14.

Borgohain T (2010) Reservoir fairway analysis of a Barail interval of Deohal area in upper Assam basin using high resolution sequence stratigraphy and seismic attributes. AAPG Annual Convention and Exhibition, New Orleans, 11–14 April 2010, pp. 965–85.

Chen KY, Duan XG, Zhang XB and Song RC (2010) Lithology identification and prediction of volcanic rocks based on 3D lithofacies modeling. *Journal of Southwest Petroleum University (Natural Science Edition)* **32**, 19–24.

Chen ZH, Mou ZB and Sun Y (2009) Characteristics and development strategies of fracture-cavity bedrock reservoirs in Baihu Oilfield, Vietnam. *Journal of Chinese and Foreign Energy* **14**, 45–49.

Cun YJ (2008) *Logging Evaluation Technology for Archean Buried Hill Reservoir in Jinzhou 25-1 South Oilfield, Bohai Sea*. Ph.D. thesis, China University of Petroleum (in Chinese). Published thesis.

Cuong TX and Warren JK (2009) Bach ho field, a fractured granitic basement reservoir, Cuu Long Basin, offshore SE Vietnam: a "buried-hill" play. *Journal of Petroleum Geology* **32**, 129–56.

Delhomme JP (1992) A quantitative characterization of formation heterogeneities based on borehole image analysis. In *Proceedings of 33th SPWLA Annual Logging Symposium*, Oklahoma City, June 1992.

Deng Q (2007) Analysis of reservoir characteristics and controlling factors in low Buried hill zone. *Journal of Inner Mongolia Petroleum Industry* **12**, 132–36.

Deng YH and Peng WX (2009) Discovery of Jinzhou 25-1S mixed granite buried hill large oil and gas field in Bohai Sea. *Journal of China Offshore Oil and Gas* **21**, 145–49.

Dou L, Wang J, Wang R, Wei X and Shrivastava C (2018) Precambrian basement reservoirs: case study from the northern Bongor Basin, the Republic of Chad. *AAPG Bulletin* **102**, 1803–24.

Dou LR, Wei XD, Wang JC, Li JL, Wang RC and Zhang SH (2015) Reservoir characteristics of granitic bedrock buried hill in Bongor Basin, Chad. Acta Petrolei Sinica 36, 897–925.

Fan JY (2019) Evolution of Tectonic Stress Field and Fault Response Characteristics in Dongying Depression. Ph.D. thesis, China University of Petroleum (in Chinese). Published thesis.

Fang Y (2016) Study on the Characteristics of PL9-1 Mesozoic Magmatic Buried Hill Reservoir in the Bohai Sea. Ph. D. thesis, China University of Petroleum (in Chinese). Published thesis.

Gao LL (2014) Structural Evolution Characteristics of Dongying Sag and Its Control on Hydrocarbon Accumulation. Ph.D. thesis, China University of Geosciences (in Chinese). Published thesis.

https://doi.org/10.1017/S001675682200053X Published online by Cambridge University Press

Ge ZD, Wang ZX, Zhu M, Pu R, Wang W and Zhang JY (2011) Study on the characteristics of Archean magmatic rock reservoir in Dongying depression. *Journal of Lithological Reservoirs* **23**, 48–52.

Gong ZS (2010) Continue to explore granite reservoirs in offshore basins in China. *Chinese Journal of Offshore Petroleum* **22**, 214–20.

Gu WX, Zhou H and Geng F (2008) Application of multivariate statistical methods in the establishment of reservoir porosity model. *Journal of Fault Block Oil and Gas Field* **3**, 58–61.

Haskell JB, Toelsie S and Mohan A (2010) Optimization of sand control for unconsolidated, shallow, and low-pressure sandstone reservoirs: a Suriname case study. In *Proceedings of Society of Petroleum Engineers Trinidad and Tobago Energy Resources Conference*, Port of Spain, June 2010, pp. 953–64.

Holdsworth RE, Trice R, Hardman K, McCaffrey KJW, Morton A, Frei D, Dempsey E, Bird A and Rogers S (2019) The nature and age of basement host rocks and fissure fills in the Lancaster field fractured reservoir, West of Shetland. Journal of the Geological Society 177, 1057–73. doi: http://doi.org/10.1144/jgs2019-142.

Hou FH, Li SZ, Wang JT, Yu JG and Lv QH (2005) Ancient buried hill faults in Zhuanghai Area, Jiyang depression. Journal of Marine Geology and Quaternary Geology 25, 69–73.

Huang JH, Tan XF, Cheng CJ, Li ZM, Ma LJ, Zhang HL and Wu YX (2016) Structural characteristics of weathering crust of granitic bedrock and its petroleum geological significance. *Journal of Earth Sciences* **41**, 2041–60.

Huang JX, Peng SM and Huang SW (2007) Integration of logging and seismic data in fluvial reservoir modeling. *Journal of China University of Mining and Technology* **1**, 126–31.

Hung VT, Yuichi S, Ronald N and Kyuro S (2019) Integrated workflow in 3D geological model construction for evaluation of CO2 storage capacity of a fractured basement reservoir in Cuu Long Basin, Vietnam. *International Journal of Greenhouse Gas Control* 90, 102826. doi: https://doi.org/10.1016/j.ijggc.2019.102826.

Ji Z (2015) Study on the Genesis of Archean Basement Reservoirs in Dongying Sag. Ph.D. thesis, Southwest Petroleum University (in Chinese). Published thesis.

Koning T (2003) Oil and gas production from basement reservoirs: examples from Indonesia, USA and Venezuela. In *Hydrocarbons in Crystalline Rocks* (eds N Petford and KJW McCafferty), pp. 83–92. Geological Society of London, Special Publication no. **214**.

Lan DZ (1984) Discussion on torsion and tilt of fault block in Bohai Bay Basin and its formation mechanism. *Journal of Petroleum Exploration and Development* **03**, 26–31.

Li B, Tian MR, Zhang F, Xu B and Wang XZ (2011a) Study on the characteristics and distribution of Archean basement rock reservoirs in Dongying Sag. *Journal of Lithologic Reservoir* **23**, 52–55.

Li BJ (2011) The natural fracture evaluation in the unconventional tight oligocene reservoirs-Case studies from CuuLong basin, southern offshore vietnam. In *Proceedings of* Society of Petroleum Engineers, SPE Asia Pacific Oil and Gas Conference and Exhibition, Jakarta, 20–22 September 2011, pp. 955–65.

Li J, Zhang JH, Han H, Zhu WB, Yang Y and Du YS (2015) Summary of exploration status, basic characteristics and prediction technology of igneous rock reservoirs. *Journal of Petroleum Geophysical Prospecting* **50**, 382–92.

Li LQ, Xiong XJ, Hou QP, Yang RQ and Chen Q (2016) Numerical simulation based on seismic attribute modeling and its application. *Journal of Chengdu University of Technology (Natural Science Edition)* **43**, 454–59.

Li SJ, He M, Zhao XL, Jin AW, Yuan LY and Yin TT (2011b) The Archaeozoic fracture development law and the significance of oil and gas reservoir in Luxi area and Jiyang depression, Shandong Province. Science and Technology Review 29, 28–31.

Li YT, Li GY, He RM and Xu WZ (2009) Practice and understanding of optimal combination of applicable seismic technology in Yitong Basin. *Journal of China Petroleum Exploration* **14**, 57–60.

Liu CH and Wang XZ (2010) Sequence stratigraphy research and exploration practice in the gentle slope zone of the continental Pan-shaped fault depression – taking the Dongying formation of Chengdao Dongpo as an example. *Journal of Special Oil and Gas Reservoir* **17**, 1–5.

Liu G, Zeng L, Han C, Ostadhassan M, Lyu W, Wang Q, Zhu J and Hou F (2020) Natural fractures in Carbonate basement reservoirs of the Jizhong Sub-Basin, Bohai Bay Basin, China: key aspects favoring oil production. *Energies* **13**, 4635.

Liu Z, Zen XB and Zhang WX (1997) The effect of structural tilt on the lake level change of Shanduan Lake Basin. *Journal of Acta Sedimentologica Sinica* **15**, 66–68.

Lu SK, Gu YX and Sun JM (2012) Reservoir characteristics of Archean in Jiyang depression and conventional logging identification. *Journal of Special Oil and Gas Reservoir* **19**, 21–24.

Ma LJ, Zheng HR and Jie XN (2005) Faulted structure and hydrocarbon migration in the central uplift belt of Dongying Sag. *Journal of Oil and Gas Geology* **2**, 246–51.

Ma N, Zhou JH and Cai WX (2017) Summary and prospect of logging evaluation methods for igneous rock reservoirs. *Journal of Energy and Environmental Protection* **2**, 24–31.

Nelson RA, Bueno E, Moldovanyi EP, Matcek CC and Azqiritxage I (2000) Production characteristics of the fractured reservoirs of La Paz field, Maracaibo basin, Venezuela. *AAPG Bulletin* **84**, 1791–809.

Nguyen-Trinh HA and Ha-Duong M (2015) Perspective of CO2 capture & storage (CCS) development in Vietnam: results from expert interviews. International Journal of Greenhouse Gas Control 37, 220–27.

Ni XL, Zhang P, Du BS and Le XF (2015) Application of frequency division inversion technology in predicting tight oil sweet spots—taking Zhahaquan Area in Qaidam Basin as an example. In *Proceedings of 2015 Geophysical Prospecting Technology Seminar of China Petroleum Society*. Beijing: China Petroleum Society, Editorial Office of Petroleum Geophysical Exploration, pp. 821–23.

Parra J, Hackert C, Richardson E and Clayton N (2009) Porosity and permeability images based on crosswell seismic measurements integrated with FMI logs at the Port Mayaca aquifer, South Florida. Lead Edge 28, 1212–19.

Place J, Géraud Y, Diraison M, Herquel G, Edel JB, Bano M, Le Garzic E and Walter B (2016) Structural control of weathering processes within exhumed granitoids: compartmentalisation of geophysical properties by faults and fractures. *Journal of Structural Geology* **84**, 102–19. doi: http://dx.doi.org/10.1016/j.jsg.2015.11.011

Qi JF, Xiao HZ and Zhang WG (2003) Structural geometry, kinematics characteristics and genetic interpretation of main boundary faults (belts) in Dongying Sag. *Journal of Petroleum Exploration and Development* **3**, 8–12.

Riber L, Dypvik H, Sørlie R, Naqvi SAAEM, Stangvik K, Oberhardt N and Schroeder PA (2017) Comparison of deeply buried paleoregolith profiles, Norwegian North Sea, with outcrops from southern Sweden and Georgia, USA — implications for petroleum exploration. *Palaeogeography, Palaeoclimatology, Palaeoecology* **471**, 82–95.

Shi H, Zhou XH, Sun SB, Wang G and Yao CH (2008) Research on reservoir development characteristics of JZS Buried Hill reservoir in Bohai Sea. Journal of Petroleum Geology and Engineering 3, 26–28, 32.

Sorenson RP (2005) A dynamic model for the Permian Panhandle and Hugoton fields, western Anadarko basin. *AAPG Bulletin* **89**, 921–38.

Tan WX, Wang JR, Deng Q, Qin L and Tan JZ (2015) Quantitative evaluation method and application of granite reservoir performance. *Journal of Offshore Petroleum Geology* **27**, 31–37.

Tang QS (2008) The Fault System and the Formation Mechanism of the Central Structural Belt in Dongying Sag. Ph.D. thesis, Zhejiang University (in Chinese). Published thesis.

Trice R (2014) Basement exploration, West of Shetlands: progress in opening a new play on the UKCS. In *Hydrocarbon Exploration to Exploitation West of Shetland* (eds SJC Cannon and D Ellis), pp. 81–105. Geological Society of London, Special Publication no. **397**.

Trice R, Hiorth C and Holdsworth R (2019) Fractured basement play development on the UK and Norwegian rifted margins. In Large Igneous Provinces and their Plumbing Systems (eds RK Srivastava, RE Ernst, KL Buchan and M de Kock). Geological Society of London, Special Publication no. 415. doi: 10.1144/sp495-2018-174.

Trinh XC, Warren JK and Bach HF (2009) A fractured granitic basement reservoir, Cuu Long basin, offshore SE Vietnam: a "buried-hill" play. *Journal of Petroleum Geology* **32**, 129–56.

Wang GM, Xiong ZH, Zhang J, Guo YH, Lin GS and Fu Y (2017) Reservoir fault characteristics in Bozhong Sag, Bohai Bay Basin and its controlling effect on reservoir formation. *Journal of Oil and Gas Geology* **38**, 62–70.

Wang JC, Dou LR, Xu JG, Wei XD, Wang ZF and Chen HZ (2018) Application of "two width and one height" seismic data in the characterization of granite buried hill reservoir—taking the Bongo Basin of Chad as an example. *Journal of Petroleum Geophysical Prospecting* **53**, 320–29.

Wang Q, Laubach SE, Gale JFW and Ramos MJ (2019) Quantified fracture (joint) clustering in Archean basement, Wyoming: application of the normalized correlation count method. *Petroleum Geoscience* **25**, 415–28.

Wang QC, Jiang H and Dai XJ (2006) Research on subtle oil and gas reservoirs in Niuxintuo Area, Liaohe depression. *Journal of Petroleum and Natural Gas* **1**, 138–39.

Wang X, Zhou XH, Xu GS, Liu PB, Gao KS and Guan DY (2015) Reservoir development characteristics and main controlling factors of the Penglai 9-1 granite buried hill large oil and gas field in the Bohai Sea. *Journal of Oil and Gas Geology* **36**, 262–70.

Wang YG, Xie D, Le YX and Liu W (2003) Application of seismic attribute analysis technology in reservoir prediction. *Journal of the University of Petroleum (Natural Science Edition)* **27**, 30–32.

Williams JJ and Augifield L (1972) Depositional environment and diagenesis of sedimentary reservoir and description of igneous reservoir. Stratigraphic Oil and Gas Fields 16, 623–32.

Xie RB (2019) Tectonic Evolution of the Central Uplift Belt in Dongying Sag. Ph.D. thesis, China University of Petroleum (in Chinese). Published thesis.

Xu FH, Wang ZW and Wang WH (2021) Evaluation of fractured–vuggy reservoir by electrical imaging logging based on a de-noising method. *Acta Geophysica* 69, 761–772. doi: https://doi.org/10.1007/s11600-021-00558-w.

Yang J (2004) Research on geotechnical characteristics of weathered Granite crust in the coast of South China. Ph.D. thesis, Xi'an University of Science and Technology (in Chinese). Published thesis.

Yang MH, Liu CY, Sun DS and Cui YL (2004) Analysis of the sedimentary framework and fault block warp in the strong extension period of the terrestrial extension basin: a case study of the middle section of the third member of Shahejie formation in Langgu Sag, Jizhong Depression. *Journal of Geological Sciences* **39**, 178–90.

Yang WC (2014) Research on Logging Evaluation Method of Carboniferous Igneous Rock Reservoir in the Northwestern Margin of Junggar Basin. Ph.D. Thesis, China University of Petroleum (in Chinese). Published thesis.

Ye XS, Wang WF, Chen SY and Dai JS (2006) Characteristics of fault activity in Dongying Sag and its controlling effect on sedimentation. Journal of Xi'an Petroleum University (Natural Science Edition) 5, 29–33, 90–1.

Zhang JC and Liu ZT (2014) Analysis and application of seismic wave group characteristics of metamorphic rock buried hill reservoir. *Journal of Fault Block Oil and Gas Field* **21**, 440–43.

Zhang LH, Pan BZ and Dan GY (2008) Evaluation of igneous rock reservoir with triple pore model. *Journal of Logging Technology* **1**, 37–40.

Zhang MX and Chen XL (2017) Optimal method for forward modeling of seismic attributes. *Journal of Heilongjiang University of Science and Technology* **27**, 627–30.

Zhang WZ, Zhang YY, Zha M, Qu ZP, Yu JQ, Zhang L and He C (2019) Genesis model and reservoir controlling effect of the twist-tension fault in Dongying Sag, Bohai Bay Basin. *Journal of Oil and Gas Geology* **40**, 262–70.

Zhang Y (2010) Research on Theory and Technology of Volcanic Rock Lithology Identification and Reservoir Evaluation. Ph.D. thesis, Jilin University (in Chinese). Published thesis.

Zhang YK, Tan HX and Li QH (2009) Analysis of main fault activity in Dongying depression. *Shandong Journal of Land Resources* **25**, 29–31.

Zhang ZZ, Zhang ZX, Peng DL, Zhou HK and Wang YZ (2014) Reservoir characteristics and influencing factors of metamorphic rock in Chengbei Gu7 buried hill, Chengdao Oilfield. *Journal of Offshore Petroleum* **34**, 22–27.

Zhou W (2016) Study on the Relationship Between weathering Crust of Bedrock and Hydrocarbon Migration and Accumulation in the Western Margin of Qaidam Basin. Ph.D. thesis, China University of Petroleum (in Chinese). Published thesis.

Zhu GY, Jin Q, Dai JX, Zhang YC, Guo YC, Zhang LY and Li J (2004) Study on the oil and gas accumulation stages and distribution law of Dongying depression. *Journal of Oil and Gas Geology* **2**, 209–14.

Zhu M, Liu Z, Liu HM, Li XK, Liang SZ, Gong JQ and Zhang PF (2020) Structural division of granite weathering crusts and effective reservoir evaluation in the western segment of the northern belt of Dongying Sag, Bohai Bay Basin, NE China. Journal of Marine and Petroleum Geology 121, 104612.

Zhu W (2012) Analysis and Application of Seismic Facies of Paleogene in LF Area. Ph.D. thesis, Yangtze University (in Chinese). Published thesis.

Zhu Y, Yu YX, Wang S and Wang Y (2018) Physical parameter model of igneous rock reservoirs and identification of oil layers: taking the Carboniferous of Chepaizi Uplift in Junggar Basin as an example. *Journal of Oil and Gas Geology* **39**, 119–28.

Zong GH, Xiao HQ, Li CB, Shi YS and Wang LS (1999) The structural evolution of Jiyang depression and its Tectonic significance. *Geological Journal of China Universities* **3**, 275–82.